Electronic Supplementary Material (ESI) for Journal of Materials Chemistry

Multi-Functional Metal-Organic Frameworks Assembled from a Tripodal Organic Linker

Sérgio M. F. Vilela,[1,2] Duarte Ananias,[1] Ana C. Gomes,[1]
Anabela A. Valente,[1] Luís D. Carlos,[3] José A. S. Cavaleiro,[2] João Rocha,[1]
João P. C. Tomé[2] and Filipe A. Almeida Paz[1],*

A contribution from

[1] *Department of Chemistry, CICECO, University of Aveiro, 3810-193 Aveiro, Portugal*
[2] *Department of Chemistry, QOPNA, University of Aveiro, 3810-193 Aveiro, Portugal*
[3] *Department of Physics, CICECO, University of Aveiro, 3810-193 Aveiro, Portugal*

Electronic Supporting Information

To whom correspondence should be addressed:

Dr. Filipe A. Almeida Paz
Department of Chemistry, CICECO
University of Aveiro
3810-193 Aveiro
Portugal

E-mail: filipe.paz@ua.pt
FAX: +351 234 370084
Telephone: +351 234 247126

Table of Contents

1. Characterization of the Organic PBU

1.2 – (Benzene-1,3,5-triyltris(methylene))triphosphonic Acid

3. Electron Microscopy Studies: EDS Mapping

4. Solid-State NMR: $[La_2(H_3bmt)_2(H_2O)_2]\cdot H_2O$

7. Photoluminescence

1. Characterization of the Organic PBU

1.1 – Hexaethyl(benzene-1,3,5-triyltris(methylene))tris(phosphonate)

Figure S1. ^{13}C NMR spectrum of the intermediate molecule hexaethyl(benzene-1,3,5-triyltris(methylene))tris(phosphonate) in $CDCl_3$.

1.2 – (Benzene-1,3,5-triyltris(methylene))triphosphonic Acid

Figure S2. ^{1}H NMR spectrum of the target molecule (benzene-1,3,5-triyltris(methylene))triphosphonic acid in DMSO-d_6.

Figure S3. ^{13}C NMR spectrum of the target molecule (benzene-1,3,5-triyltris(methylene))triphosphonic acid in DMSO-d_6.

Figure S4. ^{31}P NMR spectrum of the target molecule (benzene-1,3,5-triyltris(methylene))triphosphonic acid in DMSO-d_6.

2. Milder Hydrothermal Synthetic Conditions

100 °C + 24 h

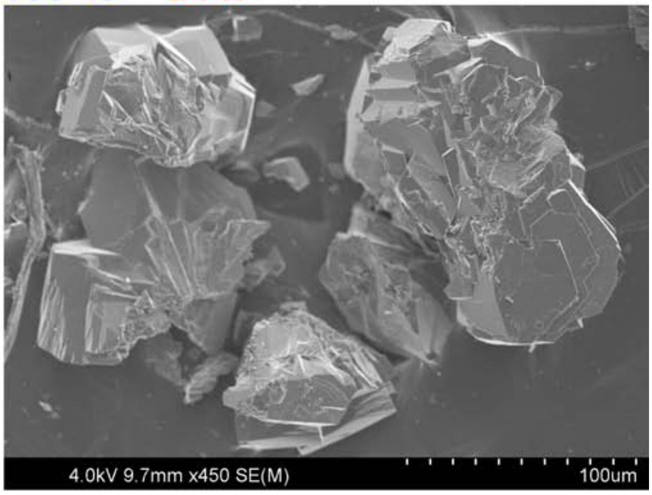

100 °C + 48 h

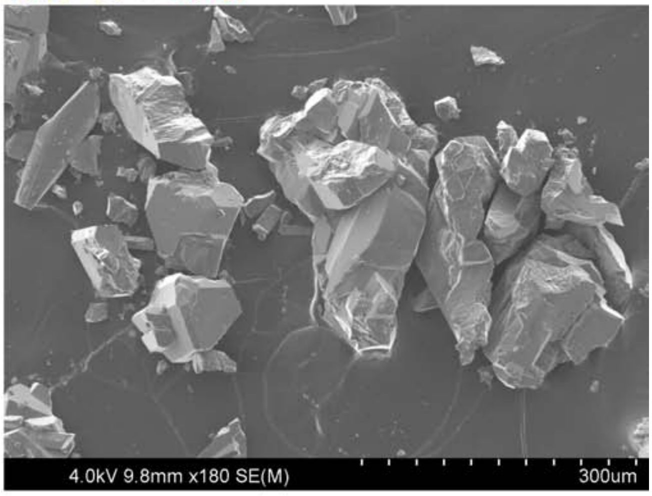

100 °C + 72 h

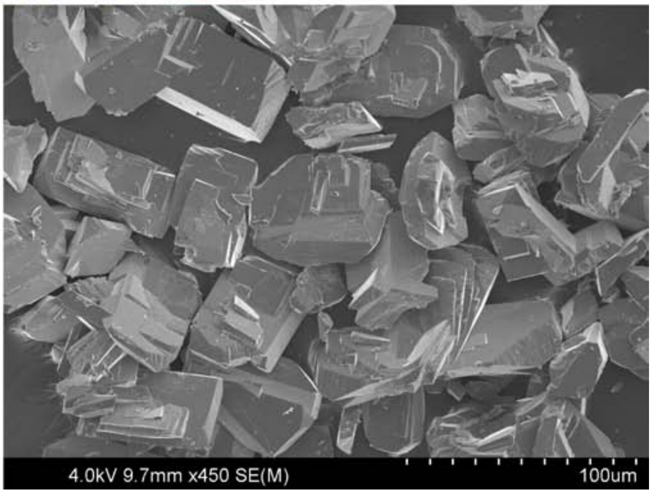

Figure S5. SEM images of the crystal morphology of the $[La_2(H_3bmt)_2(H_2O)_2]\cdot H_2O$ (**1**) material prepared at mild temperatures (100 ºC).

3. Electron Microscopy Studies: EDS Mapping

3.1 – $[(La_{0.95}Eu_{0.05})_2(H_3bmt)_2(H_2O)_2]\cdot H_2O$

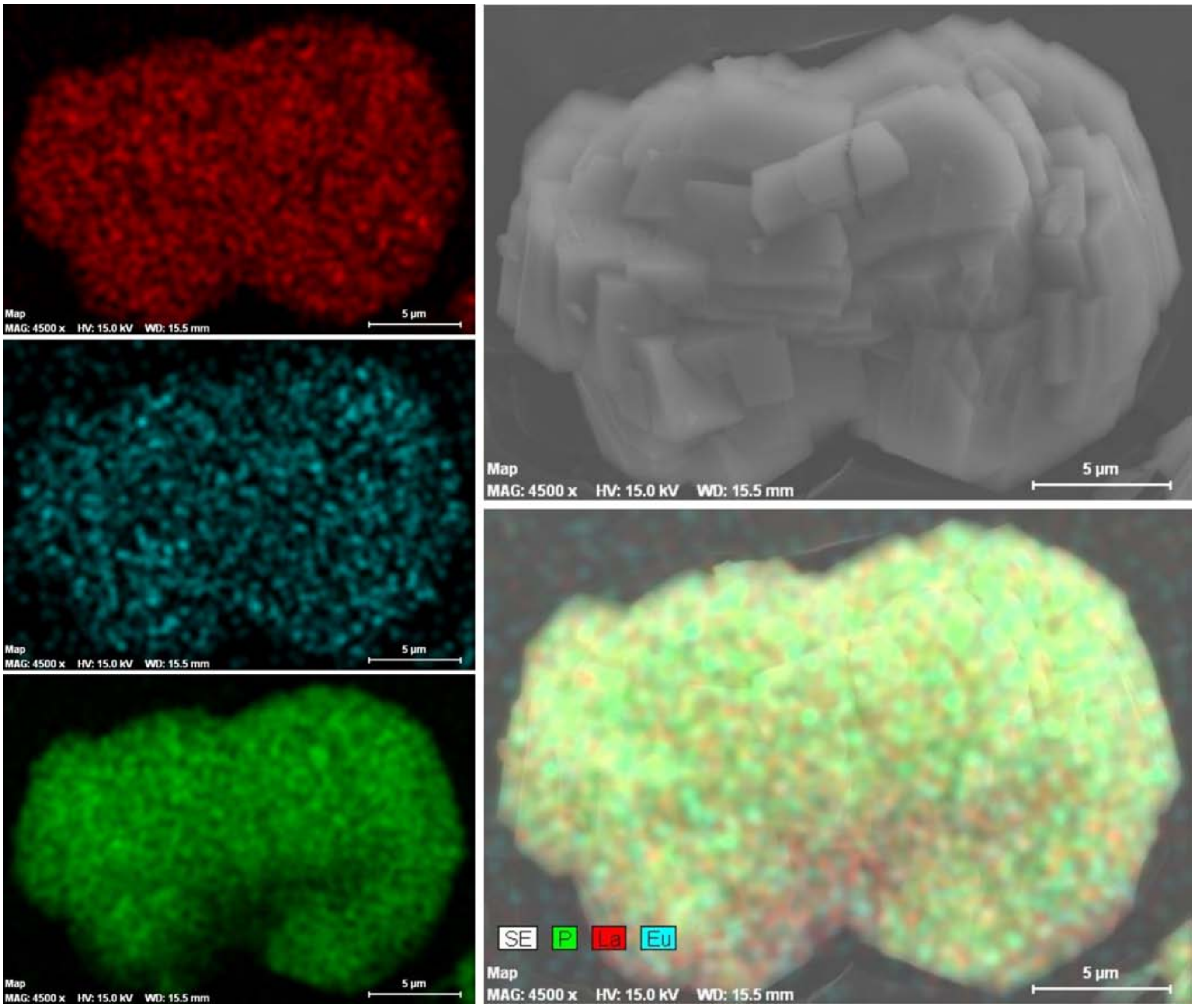

Figure S6. Electron microscopy EDS mapping studies of a portion of the $[(La_{0.95}Eu_{0.05})_2(H_3bmt)_2(H_2O)_2]\cdot H_2O$ (**5**) material.

3.2 – $[(La_{0.95}Tb_{0.05})_2(H_3bmt)_2(H_2O)_2]\cdot H_2O$

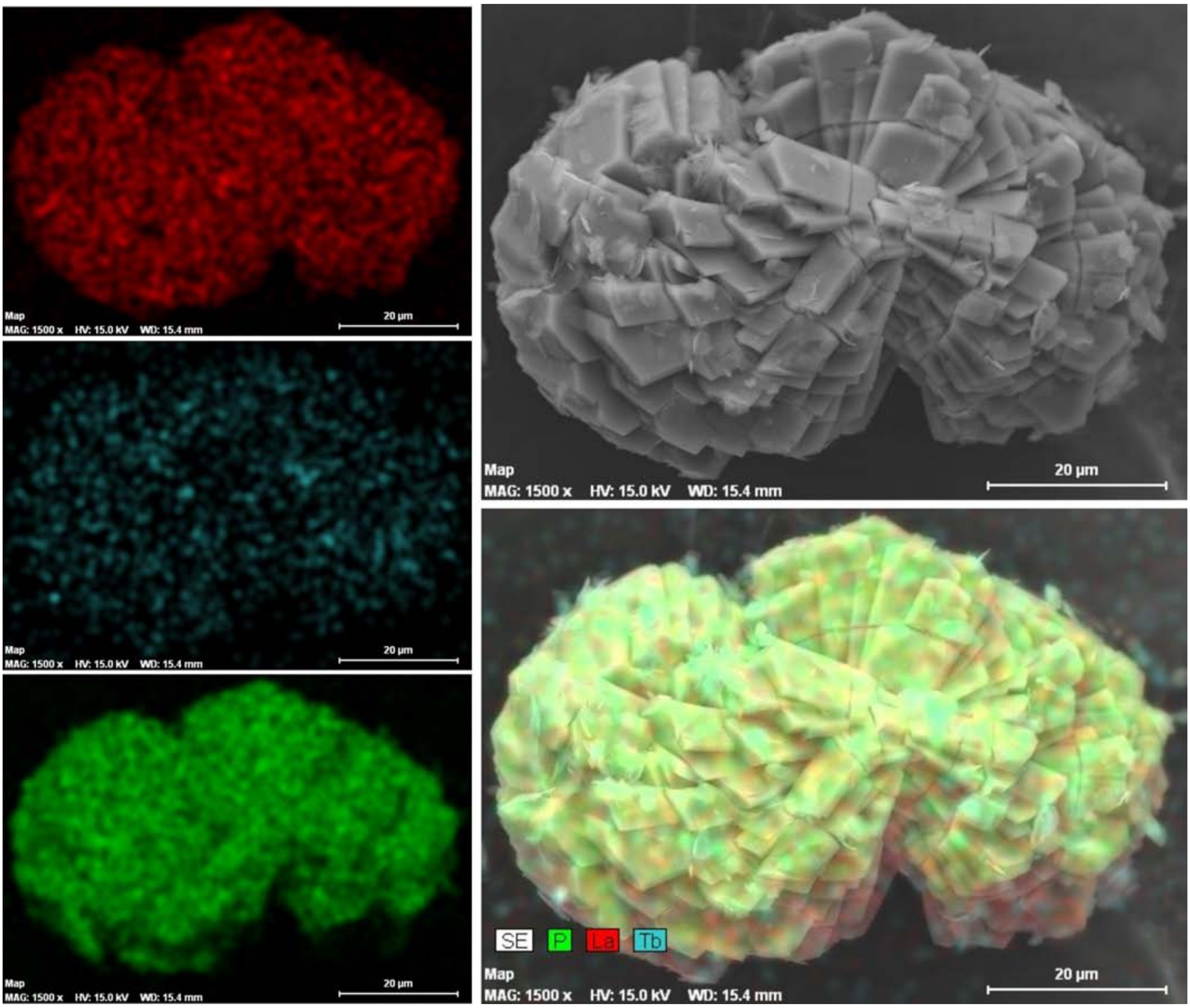

Figure S7. Electron microscopy EDS mapping studies of a portion of the $[(La_{0.95}Tb_{0.05})_2(H_3bmt)_2(H_2O)_2]\cdot H_2O$ (**6**) material.

4. Solid-State NMR: $[La_2(H_3bmt)_2(H_2O)_2]\cdot H_2O$

4.1 – $^{13}C\{^1H\}$ CP MAS

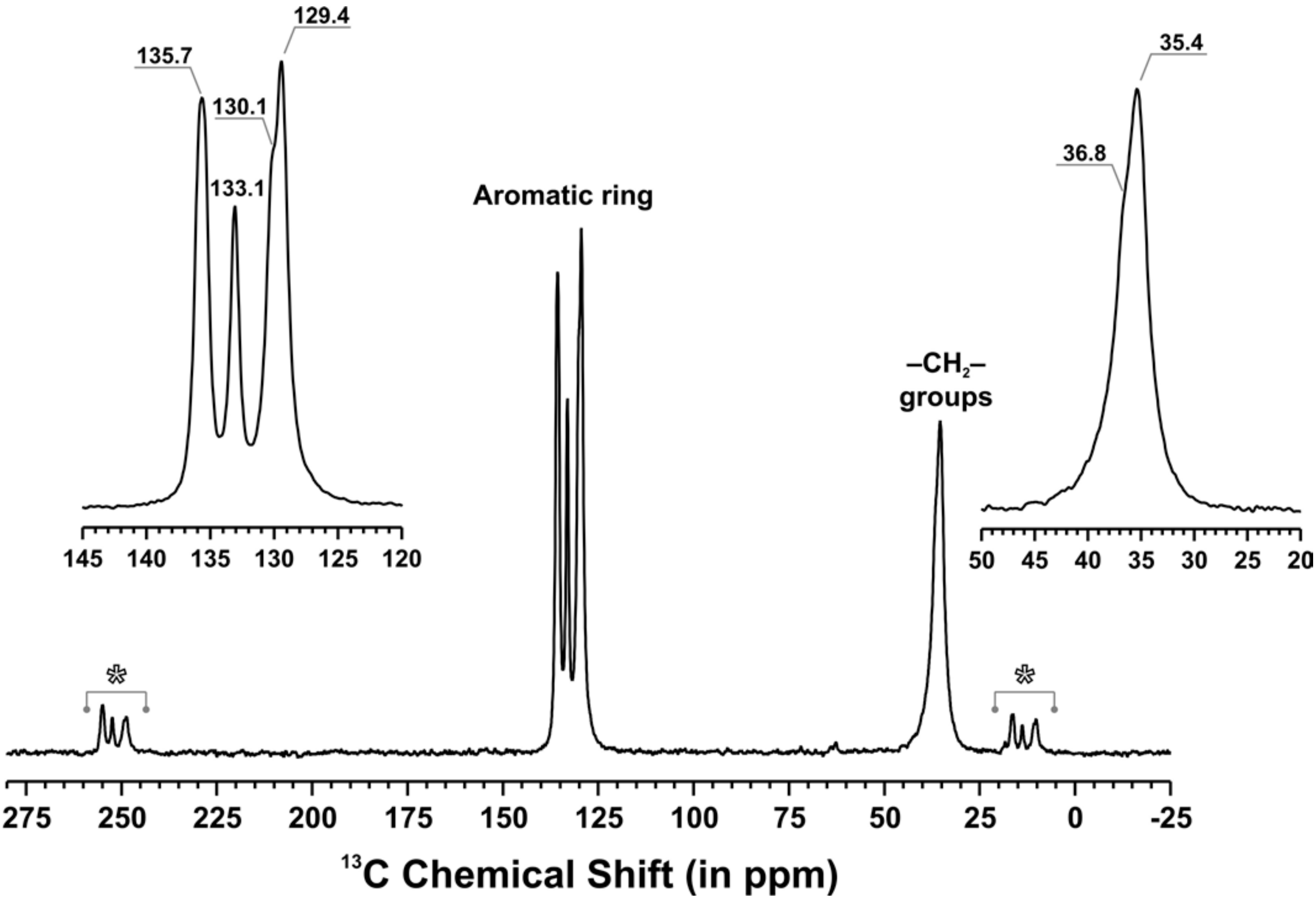

Figure S8. $^{13}C\{^1H\}$ CP MAS spectrum of $[La_2(H_3bmt)_2(H_2O)_2]\cdot H_2O$ (**1**). Spinning sidebands are depicted by an asterisk.

4.2 – ^{31}P MAS

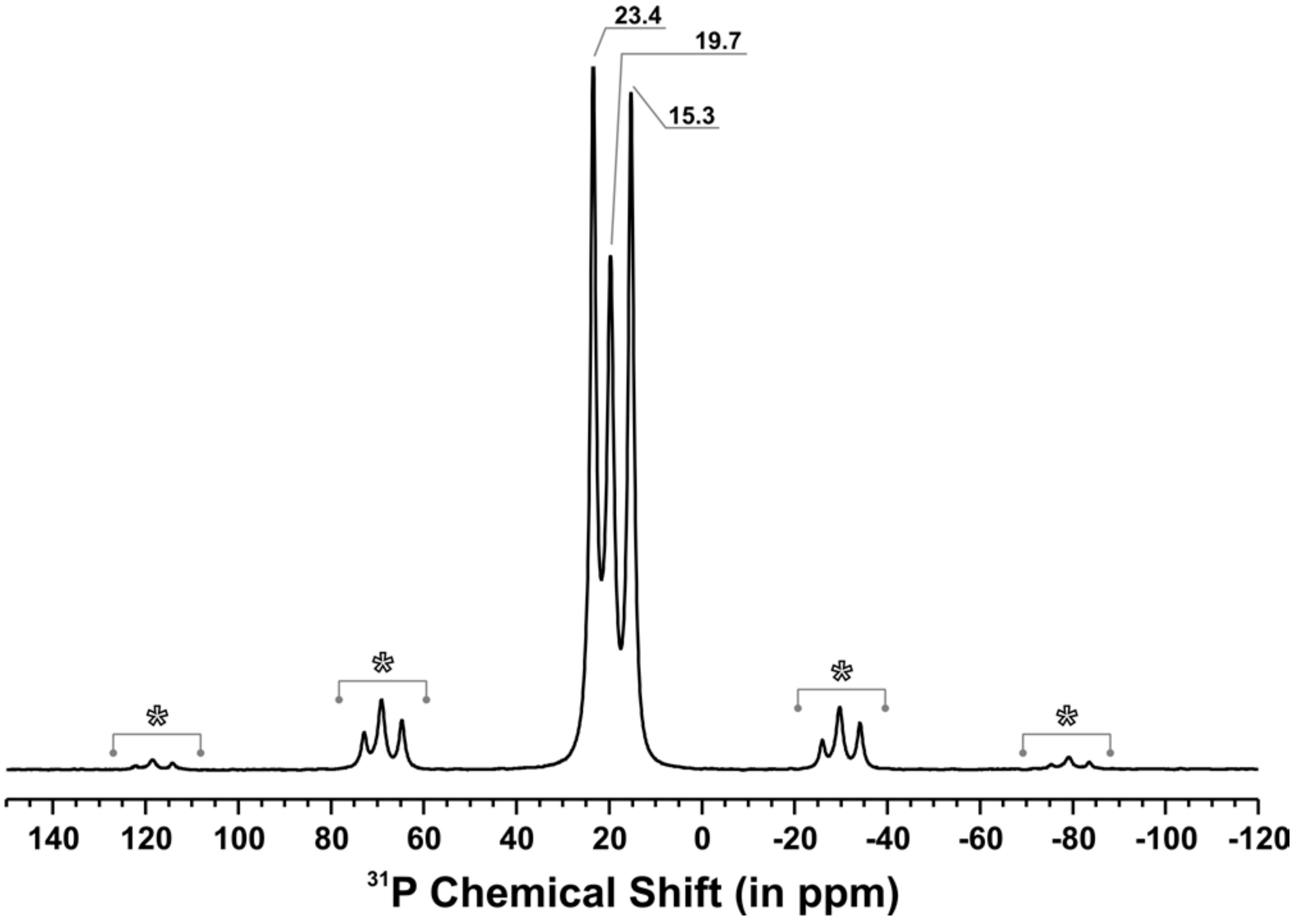

Figure S9. ^{31}P MAS spectrum of $[La_2(H_3bmt)_2(H_2O)_2]\cdot H_2O$ (**1**). Spinning sidebands are depicted by an asterisk. Peak deconvolution and integration throughout the entire spectral range (*i.e.*, including the spinning sidebands) gives a ratio of *ca.* 1.00 : 1.04 : 1.01 for the isotropic resonances at *ca.* 15.3, 19.7 and 23.4 ppm, respectively, which is in perfect agreement with the crystal structure determination of the same material.

5. FT-IR Spectroscopy

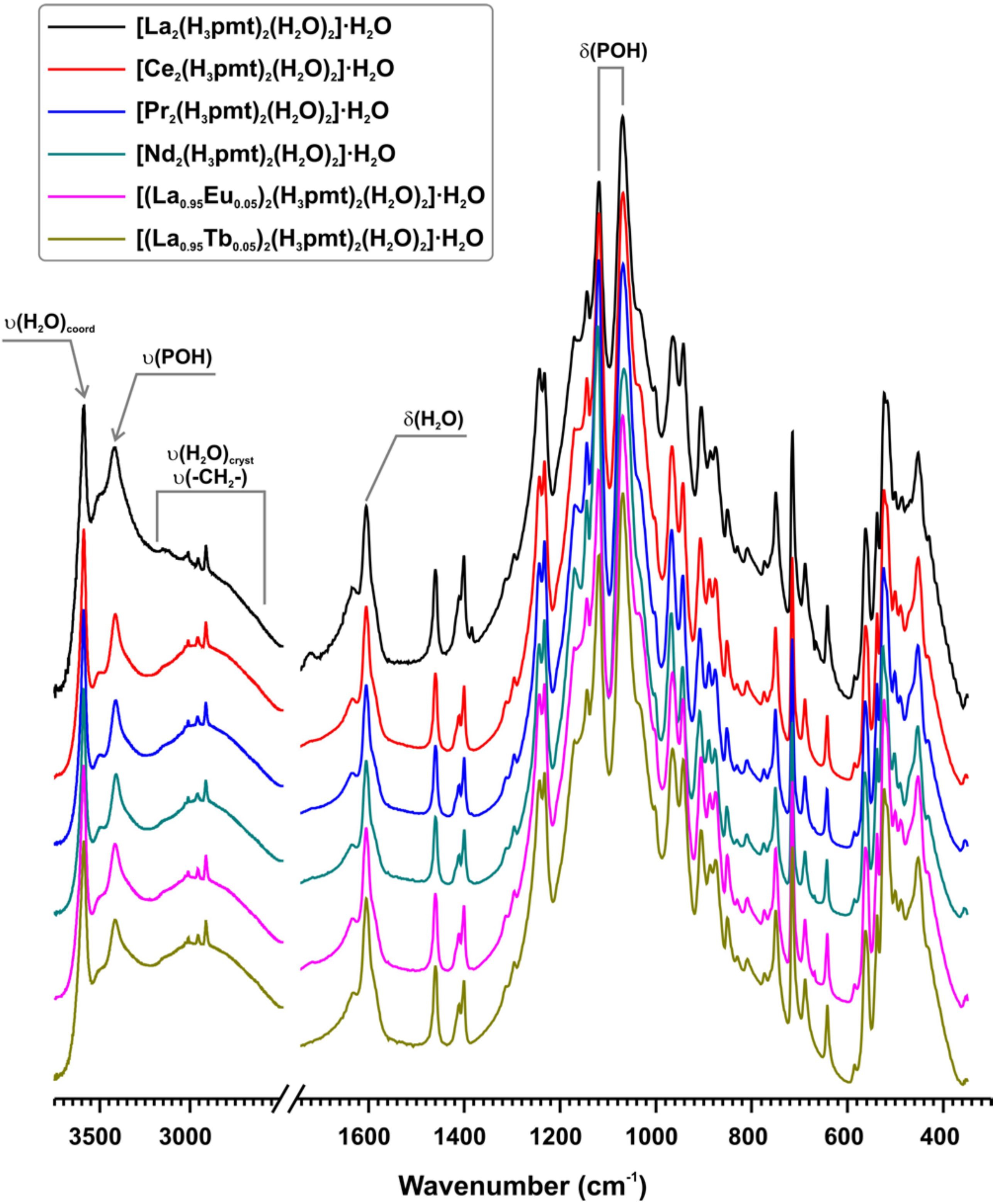

Figure S10. FT-IR spectra of the [Ln$_2$(H$_3$bmt)$_2$(H$_2$O)$_2$]·H$_2$O materials [where Ln^{3+} = La^{3+} (**1**), Ce^{3+} (**2**), Pr^{3+} (**3**), Nd^{3+} (**4**), (La$_{0.95}$Eu$_{0.05}$)$^{3+}$ (**5**) and (La$_{0.95}$Tb$_{0.05}$)$^{3+}$ (**6**)]. The most relevant and diagnostic bands associated with the structural features of the materials are depicted.

6. Thermogravimetry

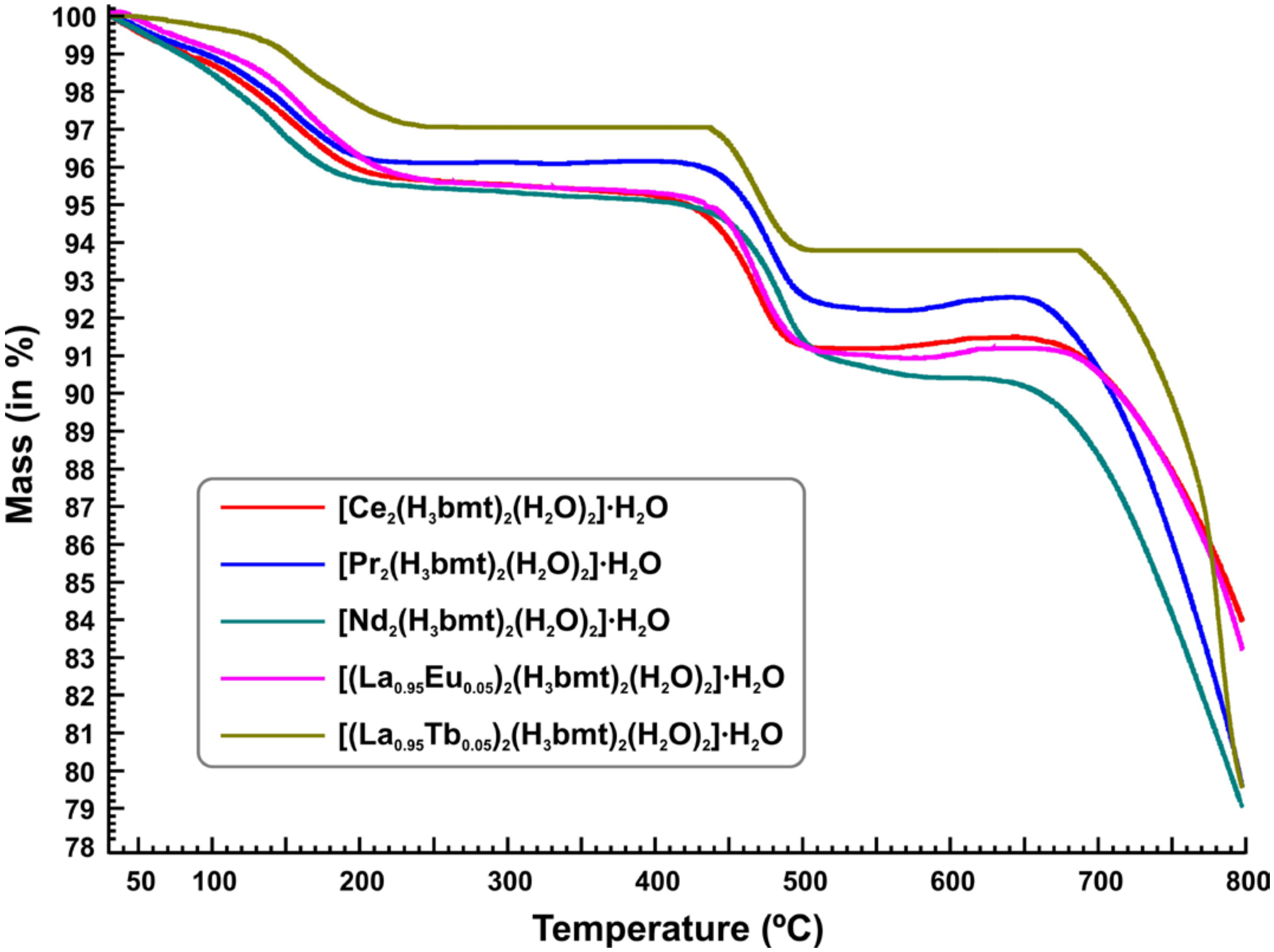

Figure S11. Thermograms of the $[Ln_2(H_3bmt)_2(H_2O)_2]\cdot H_2O$ materials [where Ln^{3+} = Ce^{3+} (**2**), Pr^{3+} (**3**), Nd^{3+} (**4**), $(La_{0.95}Eu_{0.05})^{3+}$ (**5**) and $(La_{0.95}Tb_{0.05})^{3+}$ (**6**)].

7. Photoluminescence

7.1 – Eu^{3+} Materials

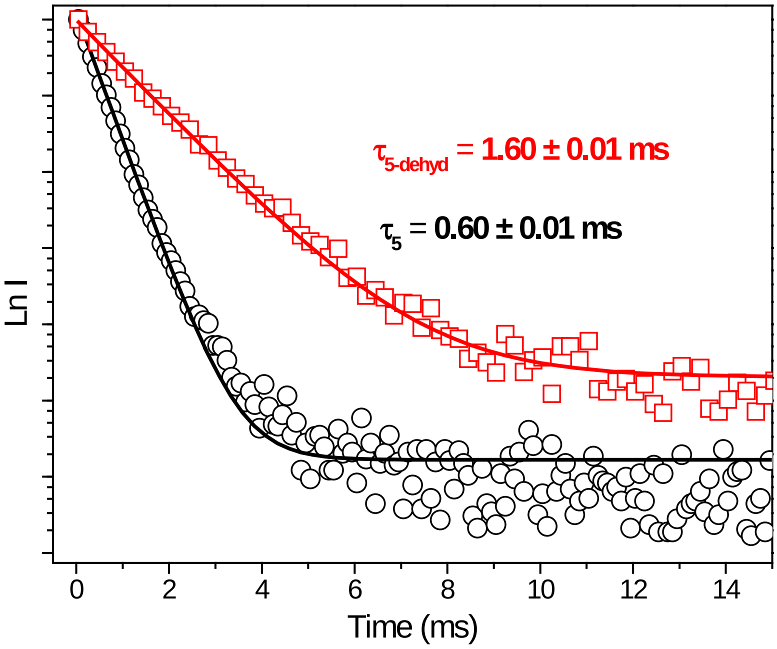

Figure S12. $^5D_0$ decay curves of $[(La_{0.95}Eu_{0.05})_2(H_3bmt)_2(H_2O)_2]\cdot H_2O$ (**5**) (**black**) and $[(La_{0.95}Eu_{0.05})(H_3bmt)]$ (**5-dehyd**) (**red**), acquired at 298 K while monitoring the emission at 611.5 and 612.1 nm, respectively. Curves were fitted by using single exponential decay functions. The excitation was performed at 393 nm.

7.2 – Tb^{3+} Materials

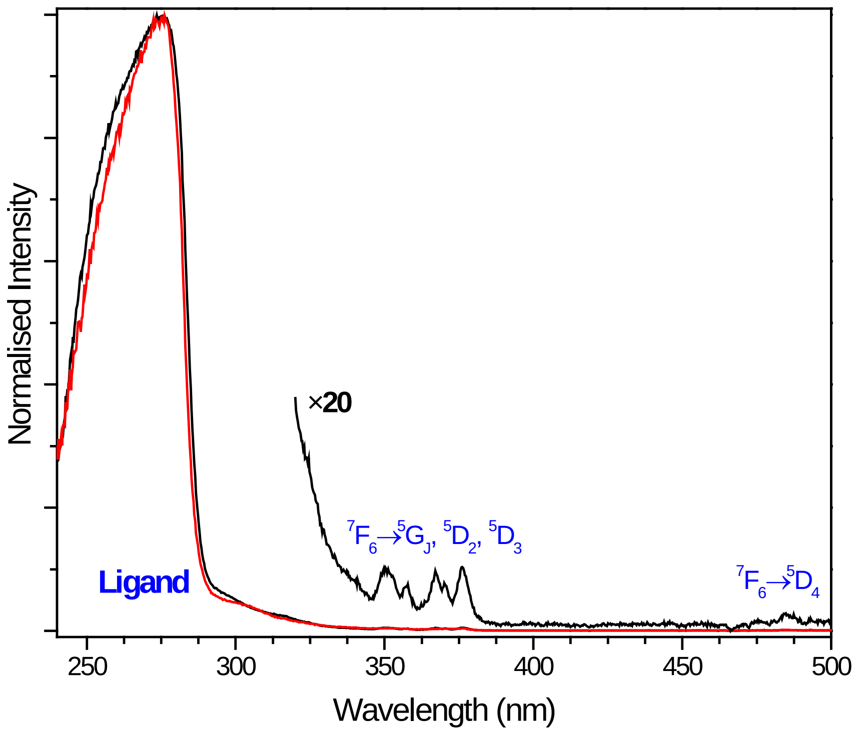

Figure S13. Excitation spectra of $[(La_{0.95}Tb_{0.05})_2(H_3bmt)_2(H_2O)_2]\cdot H_2O$ (**6**) (**black** line) and $[(La_{0.95}Tb_{0.05})(H_3bmt)]$ (**6-dehyd**) (**red** line) at 298 K while monitoring the Tb^{3+} emission at 542 nm.

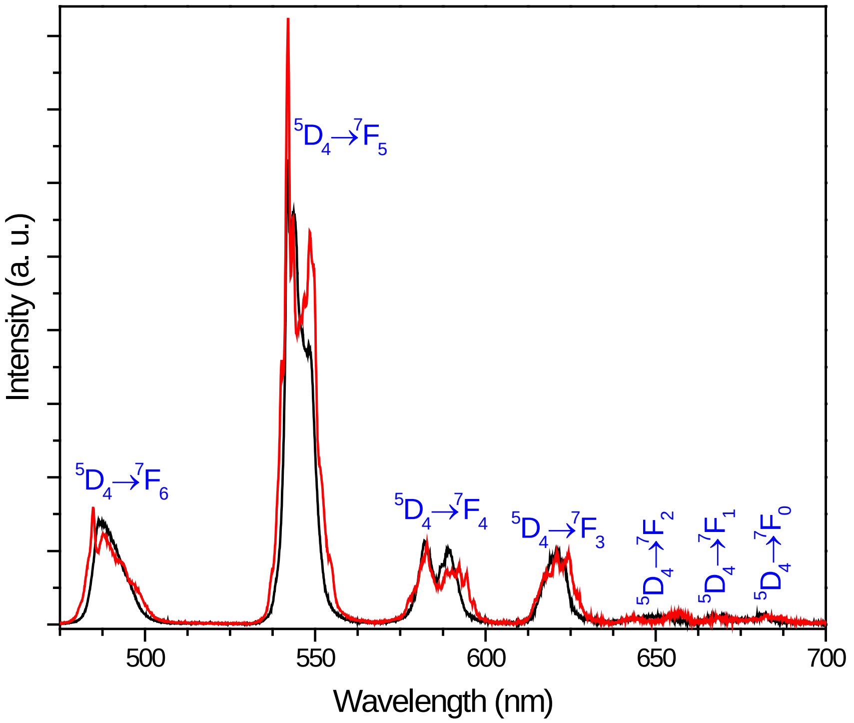

Figure S14. Ambient temperature (298 K) emission spectra of $[(La_{0.95}Tb_{0.05})_2(H_3bmt)_2(H_2O)_2]\cdot H_2O$ (**6**) and $[(La_{0.95}Tb_{0.05})(H_3bmt)]$ (**6-dehyd**) with excitation at 280 nm: **black** line, **6** at ambient pressure; **red** line, **6** after dehydration (**6-dehyd**) at 450 K under a vacuum of 5×10^{-6} mbar.

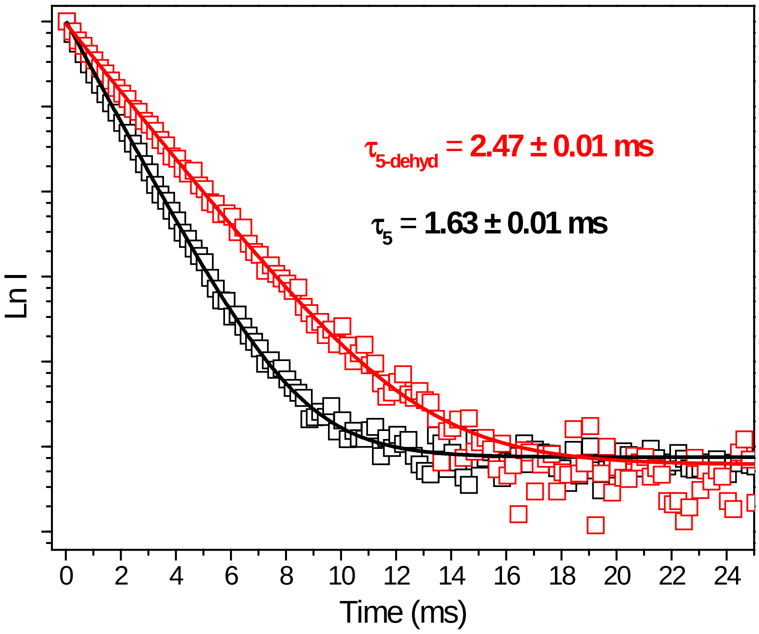

Figure S15. $^5D_4$ decay curves of $[(La_{0.95}Tb_{0.05})_2(H_3bmt)_2(H_2O)_2]\cdot H_2O$ (**6**) (**black**) and $[(La_{0.95}Tb_{0.05})(H_3bmt)]$ (**6-dehyd**) (**red**) acquired at 298 K while monitoring the emission at 542 nm. Data points were fitted using single exponential decay functions. The excitation was performed at 280 nm.

7.3 – La^{3+} Material

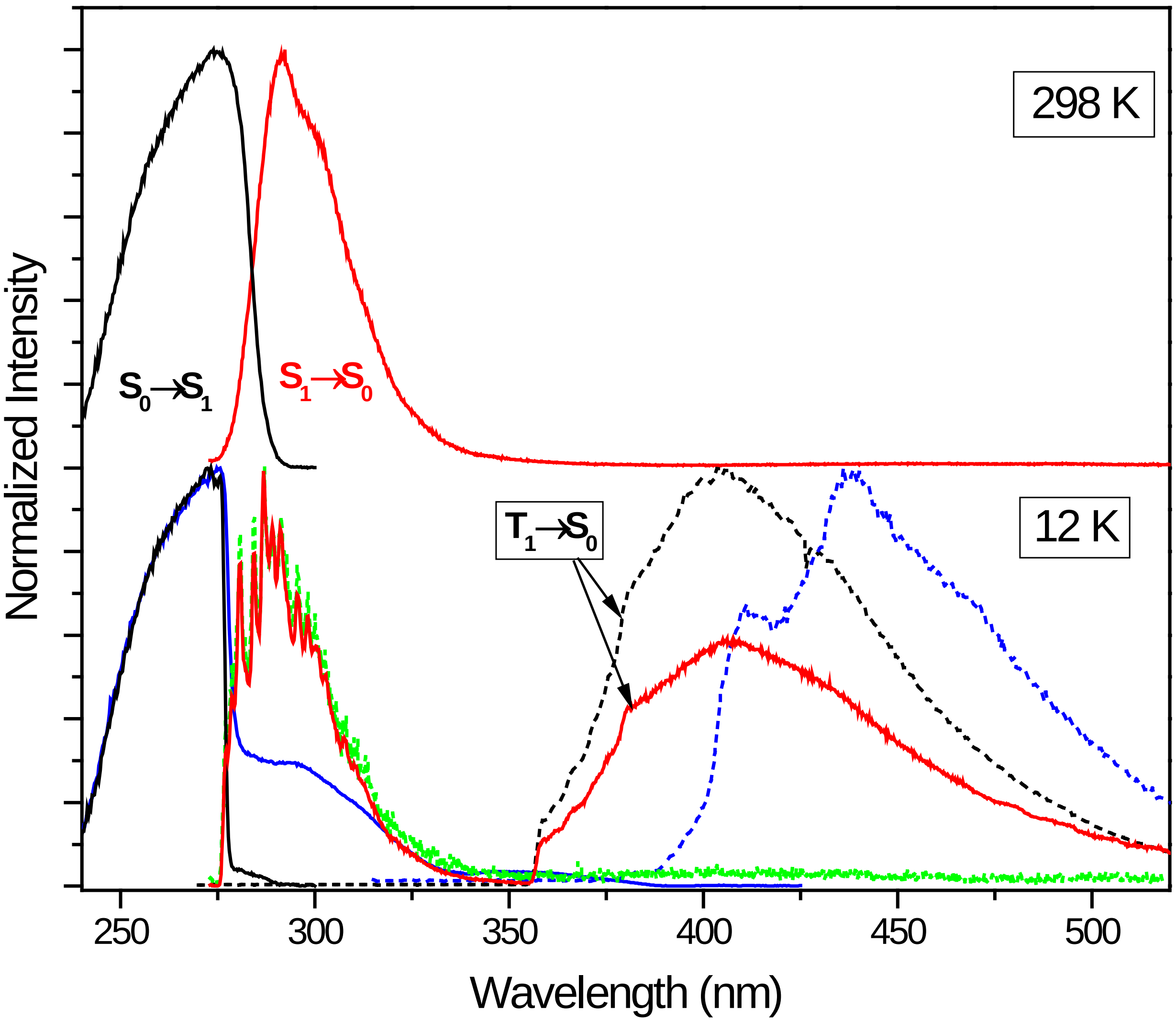

Figure S16. Excitation and emission spectra of $[La_2(H_3bmt)_2(H_2O)_2]\cdot H_2O$ (**1**) recorded at 12 K and 298 K. Stationary state spectra are depicted with solid lines; dashed lines represent time-resolved emission spectra. For the excitation spectra (stationary state) the emission was detected at 305 nm (**black** lines) and at 435 nm (**blue** lines). For the emission stationary state spectra (**red** lines) the excitation was fixed at 270 nm. Time-resolved emission spectra: dashed **green** line, initial delay 0.01 ms and integration time of 0.05 ms ($\lambda_{Exc.}$=270 nm); dashed **black** line, initial delay 0.2 ms and integration time of 30 ms ($\lambda_{Exc.}$=270 nm); dashed **blue** line, initial delay 0.2 ms and integration time of 30 ms ($\lambda_{Exc.}$=310 nm).

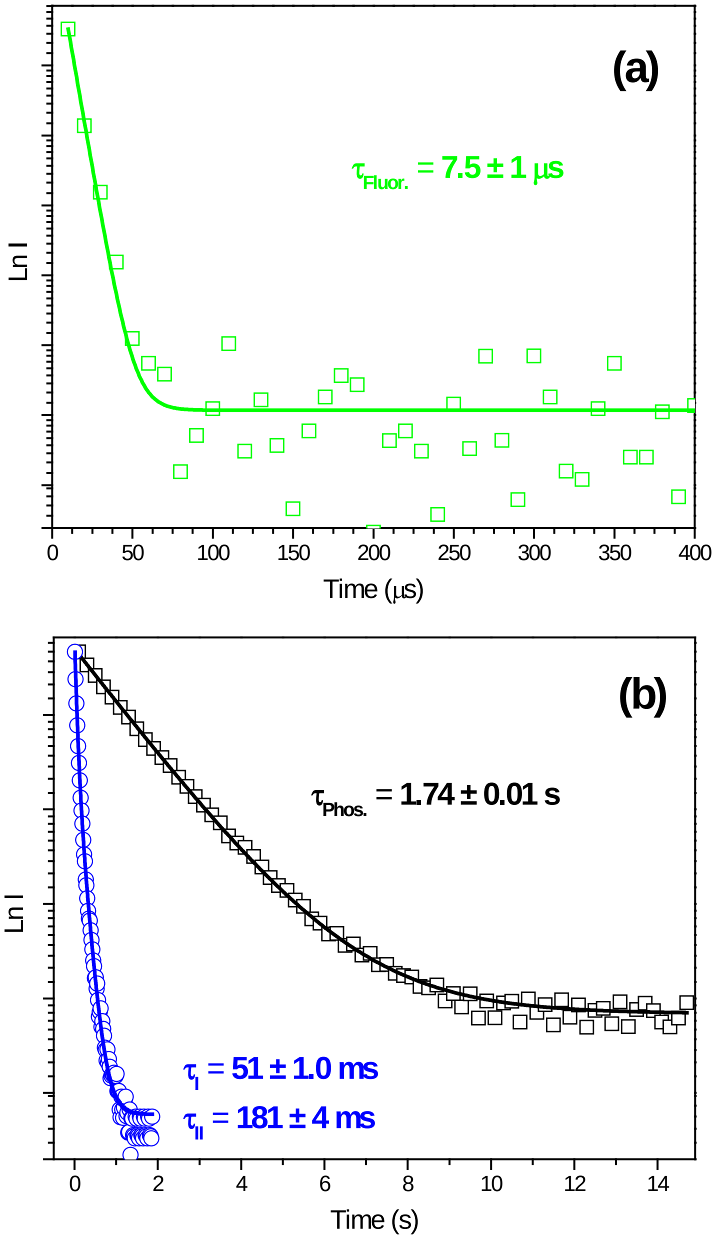

Figure S17. Time decay curves of [La$_2$(H$_3$bmt)$_2$(H$_2$O)$_2$]·H$_2$O (**1**) acquired at 12 K. (**a**) **Green** squares: fluorescence emission detected at 287 nm with the excitation fixed at 270 nm. (**b**) **Black** squares: phosphorescence emission detected at 385 nm with the excitation fixed at 270 nm. **Blue** circles: emission detected at 435 nm with excitation fixed at 300 nm. **Green** and **black** lines correspond to data fits using single exponential decay functions. The **blue** line corresponds to a data fit using a bi-exponential decay function. *Please note*: because the employed phosphorometer is unable to discriminate time values lower than 10 μs, the fitted fluorescence value and its error (calculated from the fit) can only be considered as a rough estimation of the real fluorescence lifetime.

7.4 – Quantum Efficiency and Coordinated Water Molecules Calculations

Based on the emission spectra, $^5D_0$ lifetimes and empirical radiative and non-radiative transition rates, the $^5D_0$ quantum efficiency, q,[1-3] has been determined for compounds **5** and **5-dehyd,** establishing the effect of the coordinated water molecules on the reduction of the emission efficiency. Assuming that only non-radiative and radiative processes are involved in the depopulation of the $^5D_0$ state, q is given by:

$$q = \frac{k_r}{k_r + k_{nr}} \quad \text{(Eq. 1)}$$

where k_r and k_{nr} are the radiative and non-radiative transition probabilities, respectively, and $k_{exp} = \tau_{exp}^{-1}$ $(k_r + k_{nr})$ is the experimental transition probability. The emission intensity, I, taken as the integrated intensity S of the emission lines for the $^5D_0 \rightarrow {}^7F_{0-6}$ transitions, is given by:

$$I_{i \rightarrow j} = \hbar w_{i \rightarrow j} A_{i \rightarrow j} N_i \equiv S_{i \rightarrow j} \quad \text{(Eq. 2)}$$

where i and j represent the initial ($^5D_0$) and final ($^7F_{0-6}$) levels, respectively, $\hbar w_{i \rightarrow j}$ is the transition energy, $A_{i \rightarrow j}$ the Einstein coefficient of spontaneous emission and N_i the population of the $^5D_0$ emitting level.[1-3] Because the $^5D_0 \rightarrow {}^7F_{5,6}$ transitions are not observed experimentally, their influence on the depopulation of the $^5D_0$ excited state may be neglected and, thus, the radiative contribution is estimated based only on the relative intensities of the $^5D_0 \rightarrow {}^7F_{0-4}$ transitions. The emission integrated intensity, S, of the $^5D_0 \rightarrow {}^7F_{0-4}$ transitions has been measured for compounds **5** and **5-dehyd** at 298 K.

Because the $^5D_0 \rightarrow {}^7F_1$ transition does not depend on the local ligand field of the Eu^{3+} ions (due to its dipolar magnetic nature) it may be used as a reference for the whole spectrum, *in vacuo* $A(^5D_0 \rightarrow {}^7F_1) = 14.65\ s^{-1}$,[4] and k_r is given by:

$$k_r = A_{0 \rightarrow 1} \frac{\hbar\omega_{0 \rightarrow 1}}{S_{0 \rightarrow 1}} \sum_{J=0}^{4} \frac{S_{0-J}}{\hbar\omega_{0-J}} \quad \text{(Eq. 3)}$$

where A_{0-1} is the Einstein coefficient of spontaneous emission between the $^5D_0$ and the $^7F_1$ levels. An average index of refraction of 1.5 was considered for both samples, leading to $A(^5D_0 \rightarrow {}^7F_1) \approx 50\ s^{-1}$.[5]

The number of water molecules (n_w) coordinated to Eu^{3+} and Tb^{3+} may be determined using the empirical formula of Kimura & Kato (with an intrinsic error of ±0.25) using the ambient temperature lifetimes of the as-prepared and dehydrated materials:[6]

$$n_w = A \times \left(\frac{1}{\tau_{Exp}} \right) - B \quad \text{(Eq. 4)}$$

where $A = 1.1$ and $B = 0.71$ for Eu^{3+}, and $A = 4.0$ and $B = 1.0$ for Tb^{3+}.

8. References

1. L. D. Carlos, Y. Messaddeq, H. F. Brito, R. A. S. Ferreira, V. D. Bermudez and S. J. L. Ribeiro, *Adv. Mater.*, 2000, **12**, 594-598.

2. O. L. Malta, H. F. Brito, J. F. S. Menezes, F. Silva, S. Alves, F. S. Farias and A. V. M. deAndrade, *J. Lumines.*, 1997, **75**, 255-268.

3. O. L. Malta, M. A. C. dosSantos, L. C. Thompson and N. K. Ito, *J. Lumines.*, 1996, **69**, 77-84.

4. M. H. V. Werts, R. T. F. Jukes and J. W. Verhoeven, *Phys. Chem. Chem. Phys.*, 2002, **4**, 1542-1548.

5. M. F. Hazenkamp and G. Blasse, *Chem. Mat.*, 1990, **2**, 105-110.

6. T. Kimura and Y. Kato, *J. Alloy. Compd.*, 1995, **225**, 284-287.